The expansion velocity of this shell, which can be measured from the line profile, is thought to be a diagnostic of the age of the exciting star: initially more massive and therefore shorter-lived stars give rise to larger expansion velocities. When the radio-selected sample of Lindqvist, Habing & Winnberg (1992) is divided into two according to whether the expansion velocity is greater than or less than $18\,\mathrm{km\,s^{-1}}$, the velocity dispersions of the subsamples are $\sigma_{\rm los} = 82 \pm 7\,\mathrm{km\,s^{-1}}$ for the slowly expanding (old) stars and $\sigma_{\rm los} = 65 \pm 6\,\mathrm{km\,s^{-1}}$ for the rapidly expanding (young) stars. The rapidly expanding stars are significantly more strongly concentrated towards the plane than are the slowly expanding stars. Both samples show evidence for Galactic rotation. In fact, the mean values of $\langle v_{\rm los} \times \mathrm{sign}(l)\rangle$ are very similar for this sample and for the samples of IRAS-selected OH/IR stars studied by Nakada *et al.* and te Lintel-Hekkert *et al.*, even though the Lindqvist *et al.* sample covers a much smaller range in $|l|$ ($|l| < 1°$) than do the IRAS-selected surveys.

If the transverse velocities of bulge stars exceed $100\,\mathrm{km\,s^{-1}}$, their proper motions should be measurable: $120\,\mathrm{km\,s^{-1}}$ at a distance of $R_0 = 8\,\mathrm{kpc}$ yields $3.1\,\mathrm{mas\,yr^{-1}}$. Spaenhauer, Jones & Whitford (1992) have measured proper motions for 429 stars in Baade's Window. These stars were selected to have $B - V > 1.4$, with the intention of including within the sample all K and M giants in the field.[7] The proper motions measured by Spaenhauer *et al.* are *relative*, that is, the mean proper motion of the sample is unknown. The dispersions of μ_l and μ_b within the sample are $(\sigma_l, \sigma_b) = (3.2 \pm 0.1, 2.8 \pm 0.1)\,\mathrm{mas\,yr^{-1}}$. The subsample formed by stars fainter than $B = 18$ has only very slightly larger dispersions. Since any disk stars in the sample should be relatively nearby and therefore mostly brighter than $B = 18$, this result suggests that disk contamination is not a major problem. The rough agreement between the line-of-sight and transverse velocity dispersions shows that any velocity anisotropy within the bulge is minor. It does not follow that the velocity ellipsoids (see below) within the bulge are isotropic, however, because these ellipsoids will in most places not be aligned with the direction to Baade's Window and the l and b directions.

10.3 Kinematics of stars near the Sun

10.3.1 The solar motion

We now fill a gap in our knowledge which we papered over in Chapters 2 and 9: determining the velocity of the Sun relative to the LSR. Our strategy for this project is the following. We identify a series of types of spectroscopically similar stars – gK stars, dM stars etc. – and then determine the velocity

[7] The first epoch plates were exposed by W. Baade in 1950.

of the Sun relative to the mean velocity of each type. Each such velocity is called the **solar motion** relative to that type of stars. We shall find that the solar motion varies systematically with the type studied, and that the velocity of the LSR can be inferred from this systematic variation.

The solar motion can be determined from either radial velocities or proper motions – see Jaschek & Valbousquet (1991) and Dehnen & Binney (1998a) for recent determinations by each method. To see this, let $\mathbf{v}$ denote the velocity of an object in the frame of rest of the given type; in this frame the Sun has velocity $\mathbf{v}_\odot$ and the average of any component of velocity, v_i, over stars of the type is zero. Now the heliocentric velocity of the $k^{\rm th}$ star is $\mathbf{u}_k = \mathbf{v}_k - \mathbf{v}_\odot$, so, by equation (2.23), its radial velocity is

$$v_{{\rm los}\,k} = \hat{\mathbf{x}}_k \cdot \mathbf{v}_k - v_\odot \cos\psi_k, \tag{10.7}$$

where $\hat{\mathbf{x}}_k$ is the unit vector from the Sun to the star and ψ_k is the angle between this vector and $\mathbf{v}_\odot$. When equation (10.7) is averaged over a large number of stars that are seen in almost the same direction $\hat{\mathbf{x}}$, we have that $\hat{\mathbf{x}}_k \cdot \mathbf{v}_k$ approximately averages to zero because the mean of $\mathbf{v}_k$ is, by construction, zero and $\hat{\mathbf{x}}_k \simeq \hat{\mathbf{x}}$ for all stars. Hence

$$\langle v_{\rm los}\rangle \simeq -v_\odot \cos\psi. \tag{10.8}$$

This equation states that the mean radial velocity will be largest when $\hat{\mathbf{x}}$ points in the opposite direction to $\mathbf{v}_\odot$ ($\psi = 180°$), and smallest when $\hat{\mathbf{x}}$ and $\mathbf{v}_\odot$ are parallel ($\psi = 0$) – in this direction the Sun is on the average approaching the stars, so they tend to have negative radial velocities. The direction of $\mathbf{v}_\odot$ is called the **apex of the solar motion**, and the opposite direction is called the **antapex of the solar motion**.

Suppose now that we wish to determine $\mathbf{v}_\odot$ from proper motions. We average equation (2.19) for a star's proper motion over a large number of stars of the type that are all seen near the direction of $\hat{\mathbf{x}}$ and all lie approximately at distance d, so that $|\mathbf{x}_k| \simeq d$:

$$\begin{aligned}\langle\boldsymbol{\mu}\rangle &= \left\langle \frac{((\mathbf{v}_k - \mathbf{v}_\odot)\times\hat{\mathbf{x}}_k)\times\hat{\mathbf{x}}_k}{|\mathbf{x}_k|}\right\rangle \\ &\simeq \frac{(\langle(\mathbf{v}_k - \mathbf{v}_\odot)\rangle\times\hat{\mathbf{x}})\times\hat{\mathbf{x}}}{d} \\ &= -\frac{1}{d}(\mathbf{v}_\odot\times\hat{\mathbf{x}})\times\hat{\mathbf{x}} \\ &= \frac{1}{d}(\mathbf{v}_\odot - v_\odot\cos\psi\,\hat{\mathbf{x}}).\end{aligned} \tag{10.9}$$

From this equation we may deduce the physically obvious fact that the mean proper motion of members of the type vanishes in the direction of either the apex or the antapex of the solar motion ($\psi = 0, 180°$), and is largest in the

Box 10.1: Determining $\mathbf{v}_\odot$ by Least-Squares

It is not immediately obvious from equations (10.8) and (10.9) how $\mathbf{v}_\odot$ should be determined from a given body of data. We address this problem for the case of radial velocities – a closely analogous procedure works for proper motion data (Dehnen & Binney 1998a). We start by rewriting (10.7) in the form

$$\hat{\mathbf{x}}_k \cdot \mathbf{v}_k = \hat{\mathbf{x}}_k \cdot \mathbf{v}_\odot + v_{\mathrm{los}\,k} \qquad (k = 1, \ldots, N),$$

where we assume that N stars have been observed. These N equations have infinitely many solutions, since if $\mathbf{v}_k$ and $\mathbf{v}_\odot$ solve them, so do $\mathbf{v}'_k \equiv \mathbf{v}_k + \overline{\mathbf{v}}$ and $\mathbf{v}_\odot + \overline{\mathbf{v}}$; this change corresponds to a simple boost in our reference frame. To pick out the solution of interest, we have to impose the condition that the $\mathbf{v}_k$ have zero mean. Suppose that this condition *is* satisfied in the unprimed frame. Then it is easy to see that

$$S \equiv \sum_k^N (\hat{\mathbf{x}}_k \cdot \mathbf{v}'_k)^2 = \sum_k^N (\hat{\mathbf{x}}_k \cdot \mathbf{v}_k)^2 + \sum_k^N (\hat{\mathbf{x}}_k \cdot \overline{\mathbf{v}})^2 > \sum_k^N (\hat{\mathbf{x}}_k \cdot \mathbf{v}_k)^2.$$

It follows that the desired frame is that which minimizes S. Therefore we determine $\mathbf{v}_\odot$ by minimizing $S = \sum_k^N (\hat{\mathbf{x}}_k \cdot \mathbf{v}_\odot + v_{\mathrm{los}\,k})^2$ with respect to the three components of $\mathbf{v}_\odot$. That is, we solve the three simultaneous linear equations

$$0 = \frac{\partial S}{\partial v_{\odot i}} = 2 \sum_k^N (\hat{\mathbf{x}}_k \cdot \mathbf{v}_\odot + v_{\mathrm{los}\,k}) \hat{\mathbf{x}}_{k\,i} \qquad (i = 1, 2, 3)$$

for the three components $v_{\odot i}$.

Figure 10.9 Definition of a coordinate system centered on the Sun.

perpendicular directions ($\psi = 90°$). Moreover, if we further average equation (10.9) over stars that lie in the same direction but at different distances d, it remains true that $\langle \boldsymbol{\mu} \rangle$ vanishes in the apex and antapex directions. Hence, the direction of the solar motion can be deduced from proper motions even if one does not know any stellar distances. To obtain the magnitude of $\mathbf{v}_\odot$, however, it is essential to have a distance estimate for each star in one's sample.

Box 10.1 and Problem 10.5 describe the mechanics of extracting the

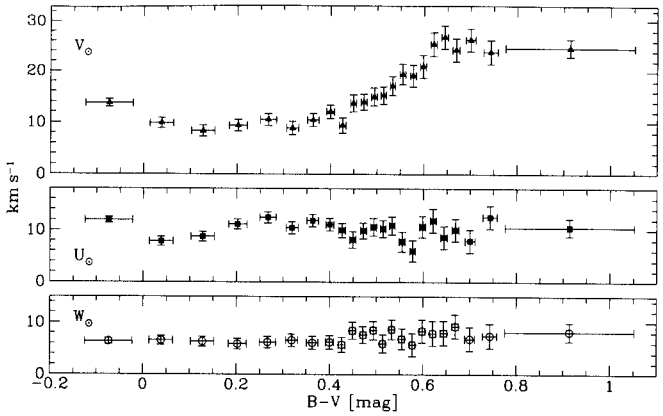

Figure 10.10 The three components of the solar motion as functions of $B - V$. [After Dehnen & Binney (1998a)]

solar motion from a large sample of stellar velocities. Figure 10.9 defines the coordinate system that is generally used in kinematic studies of the solar neighborhood. The x direction points towards the Galactic center, the direction of Galactic rotation is the y direction, and the z direction points towards the NGP. It is conventional to use the letters U, V and W for v_x, v_y and v_z, respectively. Figure 10.10 plots the U, V and W components of the solar motion relative to MS stars for which the Hipparcos satellite has determined accurate parallaxes. Different colors yield fairly similar values of $U_\odot$ and $V_\odot$, so we may estimate the radial and vertical components of the solar motion with respect to the Galactic center by averaging individual values of $U_\odot$ and $V_\odot$ in Figure 10.10. For reasons that will emerge below, we exclude the bluest data-point from this average and find the radial and vertical components of this motion to be

$$\begin{aligned} U_\odot &\equiv v_{\odot x} = 10.0 \pm 0.4\,\mathrm{km\,s^{-1}}, \\ W_\odot &\equiv v_{\odot z} = 7.2 \pm 0.4\,\mathrm{km\,s^{-1}}. \end{aligned} \qquad (10.10)$$

In Figure 10.10 it is striking that for $B - V < 0.61$, $V_\odot$ is increases steadily with increasing $B - V$, while for $B - V > 0.61$, $V_\odot$ is independent of $B - V$. Figure 10.11 shows that these variations in $V_\odot$ are linearly related to the squared random velocity S^2 for each stellar group – see Problem 10.5 for the definition of S^2. In fact, theory predicts this dependence of $V_\odot$ on S^2 – see equation (4-35) of BT. The straight line in Figure 10.11 shows a suitable linear fit to the data, with the data point for the bluest stars again excluded from the fit. From the y intercept of this line we infer the value, $5.2 \pm 0.6\,\mathrm{km\,s^{-1}}$, of $V_\odot$ for a hypothetical stellar type that had $S^2 = 0$. In §9.1 we defined the local standard of rest (LSR) as the velocity of the closed orbit within the plane that passes through the present location of the Sun.

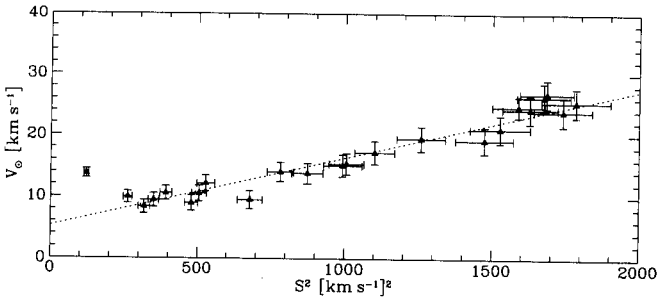

Figure 10.11 The V component of the solar motion relative to different stellar types is a linear function of the random velocity S^2 of each type. [After Dehnen & Binney (1998a)]

Since a class of stars that moved on such closed orbits would have $S^2 = 0$, we conclude that the solar motion relative to the LSR has $V_\odot = 5.2 \pm 0.6\,\mathrm{km\,s^{-1}}$. In summary, the Sun's motion relative to the LSR is

$$\left.\begin{aligned} U_\odot &= 10.0 \pm 0.4\,\mathrm{km\,s^{-1}} \\ V_\odot &= 5.2 \pm 0.6\,\mathrm{km\,s^{-1}} \\ W_\odot &= 7.2 \pm 0.4\,\mathrm{km\,s^{-1}} \end{aligned}\right\} \Rightarrow |\mathbf{v}_\odot| = 13.4\,\mathrm{km\,s^{-1}}. \qquad (10.11)$$

Thus, the Sun is moving in toward the Galactic center and up toward the north Galactic pole and away from the plane. It is also moving around the Galactic center faster than it would if it were on a circular orbit. It follows that the Sun is currently inside its guiding-center radius R_g and is approaching, but has not yet quite reached, the pericenter of its orbit – see equation (9.7) and §3.3.3 of BT for a discussion of orbits like the Sun's.

From this point on we will whenever possible refer the velocities of stars to the velocity of the LSR rather than that of the Sun. In particular, we shall assume that the means $\langle U \rangle$ and $\langle W \rangle$ vanish for stars near the Sun.

The systematic trend of $V_\odot$ with S^2 shown in Figure 10.11 is a reflection of a phenomenon called **asymmetric drift**, which is the tendency of the mean rotation velocity of a stellar population to lag behind that of the LSR more and more with increasing random motion within the population – see §10.3.2 below and §4.2.1 of BT. When the Sun's velocity is referred to such a lagging reference frame, it acquires a value of V which grows as the lag increases. It is easy to see that the magnitude of the asymmetric drift, V_a, of any stellar type is given by the difference between that type's y-coordinate in Figure 10.11 and the y-intercept of the straight line through the points. We shall see that the squared random velocity, S^2, is linearly related to $\langle U^2 \rangle$, so a linear relation holds between V_a and $\langle U^2 \rangle$. This relation takes the form

$$V_\mathrm{a} = \frac{\langle U^2 \rangle}{80 \pm 5\,\mathrm{km\,s^{-1}}} \qquad (10.12)$$

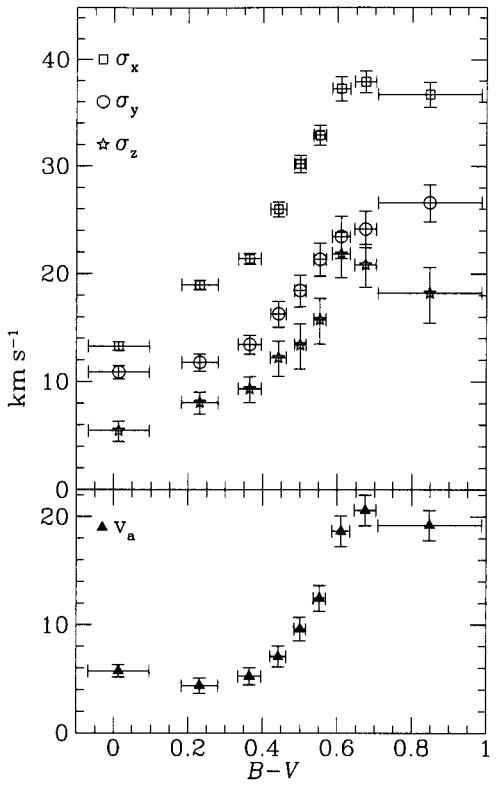

Figure 10.12 Top panel: the principal velocity dispersions σ_x, σ_y, σ_z of MS stars as a function of $B-V$. Bottom panel: the asymmetric drift, V_a, of MS stars as a function of $B-V$. [After Dehnen & Binney (1998a)]

(Dehnen & Binney 1998a). The bottom curve in Figure 10.12 shows the variation of V_a with $B-V$ for MS stars.

10.3.2 Random velocities of stars

As we have already seen, important dynamical information is contained in the dispersion of velocities,

$$\sigma_i \equiv \left\langle (v_i - \langle v_i \rangle)^2 \right\rangle^{1/2}, \qquad (10.13)$$

of each stellar type about the mean velocity of that type. The upper three curves in Figure 10.12 show, as a function of $B-V$, values for σ_x, σ_y and σ_z for MS stars. For every color we have $\sigma_x > \sigma_y > \sigma_z$. Roughly speaking, $\sigma_z \simeq 0.5\sigma_x$ while the ratio σ_y/σ_x lies in the range from 0.55 to 0.7. The fact that $\sigma_x \neq \sigma_z$ has important dynamical implications – see Chapters 3 and 4 of BT. The value of the ratio σ_y/σ_x has often been used to constrain the shape of the Milky Way's circular-speed curve – see below.

In Figure 10.12 all three velocity dispersions increase with $B-V$ color up to $B-V \simeq 0.6$ and are approximately constant redward of $B-V \simeq 0.6$,

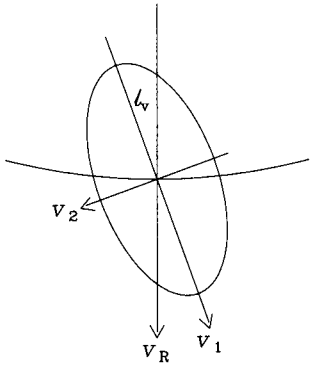

Figure 10.13 Orientation of the velocity ellipsoid. The direction to the Galactic center is upwards and the Sun lies at the center of the ellipse and moves towards the left. A portion of its orbit is shown.

just as the asymmetric drift V_a increases with $B-V$ to $B-V=0.61$ and then remains constant. From the theory of stellar evolution (§5.1), we know that MS stars bluer than $B-V\simeq 0.6$ are all younger than $\sim 10\,\mathrm{Gyr}$. In contrast, redder stars are a mixture of a few young stars and mostly old stars, and the fact that they have systematically larger velocity dispersions suggests the operation of a mechanism that leads to a progressive increase of the dispersion with time. We shall return to this idea in §10.7 below.

Vertex deviation In addition to squares of velocity components such as v_x^2, one can average products of velocity components such as $v_x(v_y-\langle v_y\rangle)$. For all stellar types, the averages of the two products of this type that involve v_z are smaller than the errors. However, for many stellar types the average of the third product, $v_x(v_y-\langle v_y\rangle)$, is significantly different from zero. Evidently for stars of these types v_x and v_y are not statistically independent: if $\langle v_x(v_y-\langle v_y\rangle)\rangle>0$, then if $v_y-\langle v_y\rangle$ is measured for some star and found to be positive, that star is more likely have a positive than a negative value of v_x. When confronted with such correlated observables, it can be helpful to find linear combinations of the observables which *are* statistically independent. Therefore we define

$$\begin{aligned} v_1 &\equiv v_x\cos l_{\rm v}-(v_y-\langle v_y\rangle)\sin l_{\rm v},\\ v_2 &\equiv v_x\sin l_{\rm v}+(v_y-\langle v_y\rangle)\cos l_{\rm v}, \end{aligned} \tag{10.14}$$

where the angle $l_{\rm v}$ is called the **vertex deviation**. Now on multiplying these equations together we find that

$$\langle v_1v_2\rangle=\tfrac{1}{2}\big(\sigma_x^2-\sigma_y^2\big)\sin 2l_{\rm v}+\big\langle v_x(v_y-\langle v_y\rangle)\big\rangle\cos 2l_{\rm v}. \tag{10.15}$$

Hence v_1 and v_2 will be statistically independent in the sense that $\langle v_1v_2\rangle=0$ if we set

$$l_{\rm v}=\tfrac{1}{2}\arctan\left(\frac{2\big\langle v_x(v_y-\langle v_y\rangle)\big\rangle}{\sigma_x^2-\sigma_y^2}\right). \tag{10.16}$$

Box 10.2: The Velocity Ellipsoid

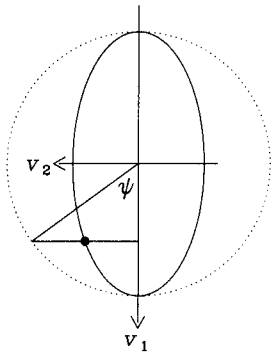

Suppose we wish to determine the mean-square speed in a direction $\hat{\mathbf{n}}$ that lies in the plane but makes an angle ψ with the v_1-direction. (The direction to the Galactic center is upwards.) Then since the velocity in the direction of $\hat{\mathbf{n}}$ is $v_n=v_1\cos\psi+v_2\sin\psi$ and $\langle v_1v_2\rangle=0$, we have

$$\begin{aligned}\langle v_n^2\rangle &= \langle v_1^2\rangle\cos^2\psi+\langle v_2^2\rangle\sin^2\psi\\ &= \langle v_1^2\rangle(\cos^2\psi+q^2\sin^2\psi),\end{aligned}$$

where q is the axis ratio of the ellipse shown in the figure. It is easy to see that the coordinates of the point marked with a blob are $(v_1,v_2)=\langle v_1^2\rangle^{1/2}\times(q\sin\psi,\cos\psi)$. Hence $\langle v_n^2\rangle^{1/2}$ is the distance from the origin to the blob.

The arctan function introduces some ambiguity in the definition of $l_{\rm v}$. By convention this ambiguity is resolved such that $\sigma_1\equiv\langle v_1^2\rangle^{1/2}>\sigma_2\equiv\langle v_2^2\rangle^{1/2}$.

The linear transformation (10.14) is a rotation of coordinates, so v_1 and v_2 are simply components of velocity in directions that are inclined by $l_{\rm v}$ to the center-anticenter direction. Figure 10.13 shows a geometrical interpretation of what is going on. If we draw the ellipse marked with semi-axes σ_1 and σ_2, then the mean-square of the component of velocity in any direction can be obtained by the construction described in Box 10.2. In fact, we can generalize this construction by replacing the circle in Box 10.2 with a sphere and the ellipse with the ellipsoidal surface that has semi-axes σ_1, σ_2 and σ_z. This surface is called the **velocity ellipsoid**. For all types of stars in the solar neighborhood, one of its principal planes coincides with the plane of the Milky Way, but its longest axis deviates from the center-anticenter direction by the vertex deviation $l_{\rm v}$. Table 10.2 gives, as a function of $B-V$, values of the σ_i and values of $l_{\rm v}$. The latter decreases with increasing $B-V$ from $\sim 30^\circ$ for the bluest stars to $\sim 10^\circ$ for stars redder than $B-V\sim 0.45$. We discuss the causes of the vertex deviation below.

Our discussion of solar-neighborhood kinematics has focused on MS stars because the largest body of accurate and homogeneous data is available for these objects. Table 10.3 shows that other stellar groups display exactly the same general kinematic trends as MS stars, however. In particular, older stellar groups are characterized by larger velocity dispersions and asymmetric drift velocities than are younger stellar groups, and vertex deviation tends

Table 10.2 Velocity dispersions and vertex deviations for MS stars

$(B-V)_{\rm min,max}$		$\sigma_1/{\rm km\,s^{-1}}$	σ_2/σ_1	σ_z/σ_1	$l_{\rm v}/{\rm deg}$
−0.238	0.139	$14.35^{+0.49}_{-0.40}$	$0.65^{+0.07}_{-0.06}$	$0.38^{+0.05}_{-0.10}$	$30.2^{+4.7}_{-5.3}$
0.139	0.309	$20.17^{+0.50}_{-0.43}$	$0.47^{+0.07}_{-0.03}$	$0.40^{+0.02}_{-0.10}$	$22.8^{+2.8}_{-3.0}$
0.309	0.412	$22.32^{+0.56}_{-0.47}$	$0.53^{+0.06}_{-0.04}$	$0.42^{+0.03}_{-0.09}$	$19.8^{+3.2}_{-3.4}$
0.412	0.472	$26.26^{+0.80}_{-0.59}$	$0.60^{+0.06}_{-0.04}$	$0.46^{+0.03}_{-0.09}$	$10.2^{+5.0}_{-5.4}$
0.472	0.525	$30.37^{+0.96}_{-0.70}$	$0.60^{+0.06}_{-0.04}$	$0.44^{+0.04}_{-0.11}$	$6.9^{+5.1}_{-5.3}$
0.525	0.582	$32.93^{+1.09}_{-0.75}$	$0.66^{+0.06}_{-0.05}$	$0.46^{+0.04}_{-0.10}$	$1.9^{+6.0}_{-6.1}$
0.582	0.641	$37.64^{+1.37}_{-0.94}$	$0.62^{+0.08}_{-0.03}$	$0.56^{+0.01}_{-0.12}$	$10.2^{+5.6}_{-6.0}$
0.641	0.719	$38.13^{+0.71}_{-0.31}$	$0.62^{+0.06}_{-0.04}$	$0.54^{+0.02}_{-0.10}$	$7.6^{+5.9}_{-6.0}$
0.719	1.543	$37.20^{+1.41}_{-0.93}$	$0.69^{+0.06}_{-0.05}$	$0.49^{+0.04}_{-0.11}$	$13.1^{+6.7}_{-7.6}$
0.610	1.543	$37.91^{+0.79}_{-0.63}$	$0.65^{+0.04}_{-0.03}$	$0.54^{+0.02}_{-0.05}$	$10.3^{+3.9}_{-3.9}$

SOURCE: Data published in Dehnen & Binney (1998a)

to decline with increasing age.

The Schwarzschild distribution Each component of the velocity distribution of, say, a population of oxygen molecules at room temperature has a Gaussian probability distribution. Schwarzschild (1907) pointed out that a similar probability distribution can account for many aspects of the probability distribution of stellar velocities. The main difference between the case of molecules in air and stars is that in the former case the velocity dispersion is independent of direction, whereas, as we have seen, in the stellar case the dispersion of a component of velocity depends strongly on direction. Schwarzschild postulated that the probability that the components of velocity (v_1, v_2, v_z) defined above lie in the element of velocity space $\mathrm{d}^3\mathbf{v} \equiv \mathrm{d}v_1\mathrm{d}v_2\mathrm{d}v_z$ is

$$P(\mathbf{v})\mathrm{d}^3\mathbf{v} = \frac{\mathrm{d}^3\mathbf{v}}{(2\pi)^{3/2}\sigma_1\sigma_2\sigma_z} \exp\left[-\left(\frac{v_1^2}{2\sigma_1^2} + \frac{v_2^2}{2\sigma_2^2} + \frac{v_z^2}{2\sigma_z^2}\right)\right]. \qquad (10.17)$$

This probability distribution is know as the **Schwarzschild distribution**. In §7.5 of BT it is shown to have a natural dynamical interpretation. Notice that P is constant on ellipsoids in velocity space.

Figure 10.14 shows the distributions in U, V and W of two samples of nearby stars for which accurate radial velocities and Hipparcos parallaxes are available.[8] The upper panels are for MS stars bluer than $B - V = 0.34$ – these are mostly A stars. The lower panels are for K and M dwarfs from Vyssotsky (1963). From the shapes of the upper histograms it is plausible that the Schwarzschild distribution gives a reasonable model of the velocity

[8] See Jahreiss & Wielen (1997) for details of these samples.

Table 10.3 Kinematics of non-MS stars

Stellar type	Asymm. drift, $V_{\rm a}$	Dispersions σ_R	σ_ϕ	σ_z	Vertex dev., $l_v(^\circ)$
Giants					
A	6.4	22	13	9	27
F	13.3	28	15	9	14
G	5.9	26	18	15	12
K0	13.4	31	21	16	14
K3	11.5	31	21	17	4
M	13.1	31	23	16	7
Supergiants					
Classical Cepheids	6.8	13	9	5	–
O–B5	8.2	12	11	9	36
F–M	6.5	13	9	7	18
Other					
Carbon stars	27	48	23	16	–
Subgiants	23	43	27	24	–
Planetary Nebulae	24	45	35	20	–
White Dwarfs	32	50	30	25	–
Variables, $P > 300^{\rm d}$	22	50	40	30	–
Variables, $P < 300^{\rm d}$	37	80	60	60	–
RR Lyrae, $P < 0.45^{\rm d}$	26	45	40	25	–
RR Lyrae, $P > 0.45^{\rm d}$	220	160	100	120	–
Subdwarfs	145	100	75	50	–

SOURCE: From data published in Delhaye (1965)

distributions of the A stars. However, from the shape of the lower histogram of V components it is clear that Schwarzschild's model cannot provide an adequate representation of the data for stellar types that have higher velocity dispersions, such as M dwarfs. Specifically, it is inherently unable to reproduce the characteristic asymmetry of the measured distribution of V components: whereas the distribution cuts off sharply at positive V, it has a long tail towards negative V.

The origin of this asymmetry in V is easy to understand. Solar-neighborhood stars with negative V have less tangential motion than is required to be on a circular orbit at R_0. Hence they are closer to apocenter than pericenter, and we may think of them as being at home interior to the solar circle. Moreover, the smaller a star's value of V is, the further inside R_0 its home lies. Now from §4.4 we know that the surface densities of galactic disks increase exponentially towards the center. Moreover, in §11.3.2 we shall find that the velocity dispersions within a disk also increase exponentially as we move inwards. For both these reasons we expect many more stars to visit us

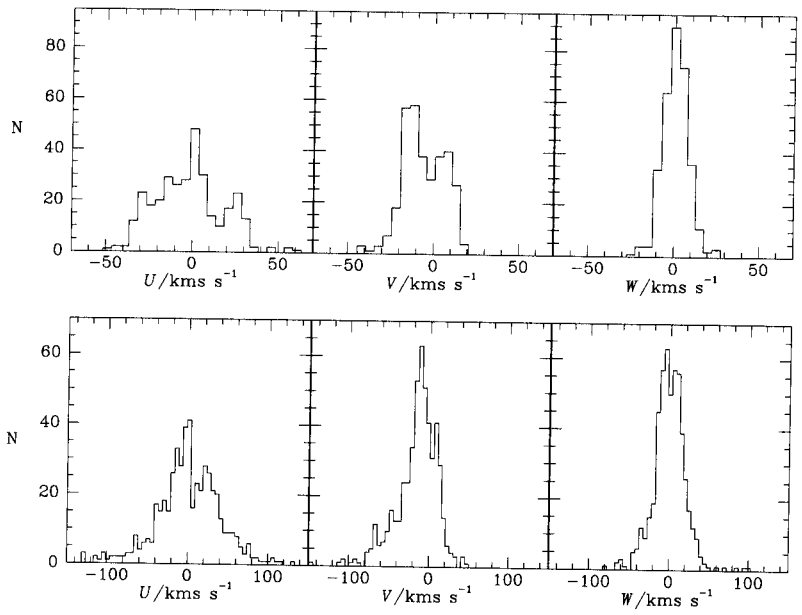

Figure 10.14 Upper panels: histograms of U, V and W for a sample of 323 nearby MS stars of MK type F1 and earlier. Lower panels: similar data for 510 K and M dwarfs. Velocities are with respect to the LSR that is defined by equations (10.11). [From data kindly supplied by H. Jahreiss]

in the solar neighbourhood from small radii than from large radii: not only does the density of tourists increase inwards, but so does the size of their travel budgets and therefore the distance from which they can visit us. The skewness of the V distributions in Figure 10.14 is simply a reflection of these basic facts.[9] The asymmetric drift discussed above is another consequence of these facts, for the skewness of the V distribution drags the mean value of V for a stellar type to more and more negative values the larger the type's velocity dispersions and therefore the skewer its V distribution.

Star streams Figure 10.15 shows the densities of MS stars of various colors in the (U, V) plane. Each panel is for a different range in $B-V$, with the bluest and youngest stars at top left and the reddest and oldest stars at bottom right. We can immediately recognize in these plots phenomena with which we are already familiar.

1. As one proceeds to redder groups, the distribution of stars spreads. The increase in the σ_i with $B-V$ quantifies this phenomenon.
2. Three of the maps show a clear tendency for the region of highest stellar density to be elongated along a line that slopes from bottom left to top right. The vertex deviation quantifies this effect.

[9] For mathematical models of the V distributions, see Cuddeford & Binney (1994).

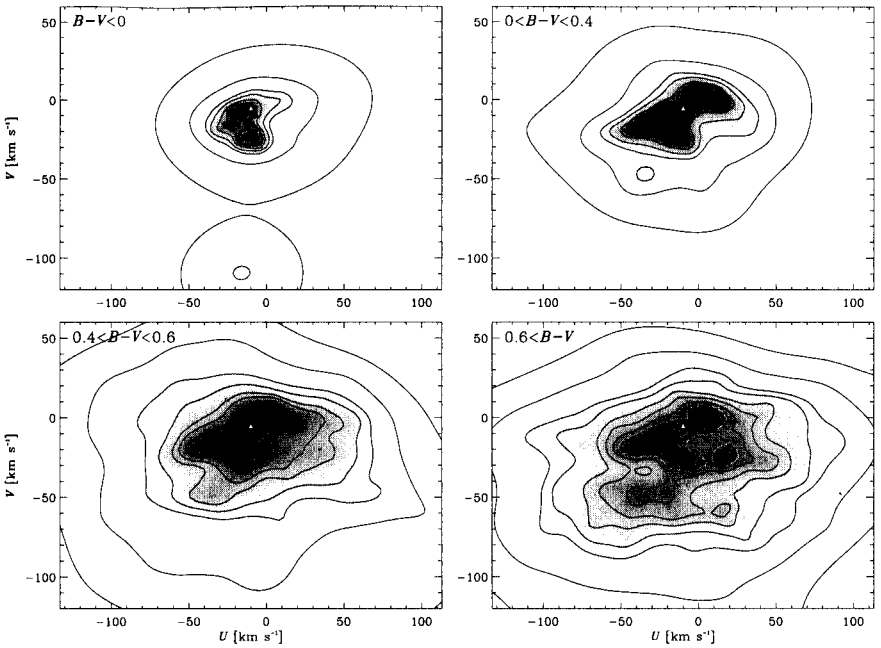

Figure 10.15 The density of stars near the Sun in velocity space. Each panel shows the density of MS stars projected onto the (U, V) plane for a different range of $B-V$ color, with the bluest stars at top left and the reddest stars at bottom right. The Sun's velocity is at $U = V = 0$ and the velocity of the LSR that is defined by equations (10.11) is marked by a triangle. [After Dehnen (1998) from data kindly supplied by W. Dehnen]

3. The lower two distributions clearly peak at $V < 0$ and extend further to negative V than to positive V. The asymmetric drift and the skewness of the V distributions in Figure 10.14 reflects this asymmetry.

In addition to these familiar phenomena, the maps of Figure 10.15 reveal the presence of tight clumps of stars in velocity space over and above the large-scale structure that the Schwarzschild distribution reproduces. In this connection, it is important that in Figure 10.15 each map is constructed from a separate sample of stars. Consequently, structure that is present in more than one map is almost certainly real rather than an artifact introduced by sampling noise.

The top right-hand panel of Figure 10.15 shows four strong peaks in the stellar density. The peak at $(U, V) = (-10, -5)\,\mathrm{km\,s^{-1}}$ is associated with the LSR, which is marked with a triangle. The peak at $(U, V) = (9, 3)\,\mathrm{km\,s^{-1}}$ corresponds to the **Sirius stream**, that at $(-12, -22)\,\mathrm{km\,s^{-1}}$ to the **Pleiades stream** and that at $(-35, -18)\,\mathrm{km\,s^{-1}}$ corresponds to the **Hyades stream**. Careful examination of the lower two panels of Figure 10.15 reveals that several wiggles and lumps that might be dismissed as noise if they occurred in only one plot, are evident in both plots and therefore probably

reflect real concentrations of stars – examples are evident near $(U,V) = (-40,-45), (15,-60)$ and $(0,-100)\,\mathrm{km\,s^{-1}}$.

These streams, or **moving groups** as they are often called, are thought to be vestiges of the clusters and associations in which most stars form (§6.2.2). Long after their stars have drifted far apart and they are no longer easily distinguishable by their space concentration, the U and V velocities of their stars remain very similar and betray the stars' common origin. Conclusive proof of this common origin comes from the fact that when all the stars of a moving group are plotted in a CM diagram, one sees the characteristic structure of the CM diagram of a coeval cluster (§6.2.2 and Eggen 1965).

Given these facts, one would expect moving groups to be most important for young stars and therefore most apparent in the distribution of early-type stars. This expectation is borne out by Figure 10.15, the top left panel of which, for stars bluer than $B-V=0$, is dominated by just two moving groups. Moreover, the brightest early-type stars in the night sky do not lie in the Galactic plane, but rather are found in **Gould's belt** in a plane inclined by about 16°. A detailed kinematical analysis of these stars (Lesh 1968) suggests that they form an expanding group.

Interestingly, Dehnen (1998) shows that star streams do not show up clearly in plots that involve the vertical component of velocity, W. This fact presumably arises because the Galactic potential changes most rapidly in the vertical direction with the consequence that as the stars of an association drift apart, they experience significantly different vertical forces when they are still subject to very similar radial and azimuthal forces. Clearly, once two stars experience very different vertical forces, their vertical velocities rapidly move apart.

Causes of vertex deviation If we imagine our Galaxy to be an axisymmetric system in a steady state in which stars are distributed at random in their orbits, then, from considerations of symmetry alone, we would expect to find one axis of the velocity ellipsoid of stars in the Galactic plane pointing exactly at the Galactic center. This expectation is borne out by dynamical theory (see BT §7.5), but, as was mentioned earlier, the vertex deviation, $l_{\rm v}$, often differs significantly from zero.

The existence of moving groups is significant for our understanding of the vertex deviation for the following reason. If a significant fraction of the objects upon which the numbers in Table 10.2 are based are, in fact, members of a few distinct moving groups, then the number of truly independent velocities employed is strongly reduced, and the statistical errors in the results will be seriously underestimated. In these circumstances, estimates of the orientation of the velocity ellipsoid axes and the velocity dispersion along these axes will be noisy. For example, if in Figure 10.15 the Pleiades stream lay at $(+12,-20)\,\mathrm{km\,s^{-1}}$ rather than at $(-12,-20)\,\mathrm{km\,s^{-1}}$, the vertex deviation would be drastically reduced, especially for stars bluer than $B-V=0.6$.

It is not clear, however, that moving groups are entirely responsible for the non-zero values of $l_{\rm v}$ in Table 10.2. A significant additional cause of vertex deviation could be the non-axisymmetric component of the Galactic potential. In §4.4.6 we encountered evidence that spiral structure affects the distribution of old as well as young stars, and in §8.2.3 we saw how the resulting spiral perturbation in a galaxy's gravitational potential imposes a pattern on the velocity field of the ISM. The velocities of stars must also be changed by the same spiral gravitational field. One can show that stellar types with small random velocities will suffer larger velocity changes than types with large velocity dispersions – see §6.2 of BT. One may also show that the spiral field will produce a vertex deviation (Kuijken & Tremaine 1994). Thus observations of spiral structure and dynamics together predict that all stellar types will show a vertex deviation, but that this will be largest for stellar types with low velocity dispersions, just as is observed. It is not yet clear whether spiral structure can account satisfactorily for all the observed vertex deviations, or whether moving groups also play an important rôle.

10.3.3 The Oort constants

Before we go on to discuss correlations between the kinematic properties of stars and their ages and chemical compositions, we should plug a gap in our discussion. This gap concerns differential rotation within the solar neighborhood. We have proceeded above as though the solar neighborhood is of negligible size compared to the Milky Way, so that one standard of rest applies throughout. Actually, the 'solar neighborhood' must be considered to be a sphere large enough to contain an adequate sample of whatever stars are under investigation. If these stars are intrinsically rare, for example most kinds of giants, the sphere may have to have a non-negligible radius and the effects within it of differential rotation may be significant.

We now show how these effects may be quantified and thus allowed for in kinematic studies. One valuable spin-off of the analysis will be evidence that the mean motion at each point of the disk is circular rather than significantly elliptical, for example. Another will be important information regarding the circular-speed curve of the Milky Way.

By analogy with the definition of the LSR (see §9.1), we associate a **standard of rest (SR)** with any point in the disk: $\mathbf{v}_{\rm SR}(\mathbf{x})$, is the velocity at $\mathbf{x}$ of the closed orbit that passes through $\mathbf{x}$. With this definition, $\mathbf{v}_{\rm LSR} = \mathbf{v}_{\rm SR}(\mathbf{x}_\odot)$. If the Milky Way were axisymmetric, $\mathbf{v}_{\rm SR}$ would be everywhere perpendicular to the local direction to the Galactic center and equal in magnitude to the local circular speed $v_{\rm c}(R)$.

By a direct extension of the logic employed in §10.3.1, we argue that at any point in the disk, $\mathbf{v}_{\rm SR}(\mathbf{x})$ should lie close to the mean velocity at $\mathbf{x}$ of any stellar type that has small random velocities. Hence key information regarding $\mathbf{v}_{\rm SR}$ can be gleaned from studies of the proper motions and radial

velocities of stars near the Sun. With this idea in mind, we now ask how the variation of $\mathbf{v}_{\rm SR}$ from point to point will be reflected in the pattern of radial velocities of stars near the Sun.

Let $\delta\mathbf{v}(\mathbf{x}) \equiv \mathbf{v}_{\rm SR}(\mathbf{x}) - \mathbf{v}_{\rm LSR}$ and let the (x, y, z) coordinate system be defined as in Figure 10.9. Each of the two components of $\delta\mathbf{v}$ is a function of the two variables (x, y) and may be Taylor expanded about the origin of the (x, y) system. Since $\delta\mathbf{v}$ vanishes at the origin by construction, we may write this series in the form

$$\begin{aligned}\begin{pmatrix}\delta v_x\\ \delta v_y\end{pmatrix} &= \begin{pmatrix}\dfrac{\partial\delta v_x}{\partial x} & \dfrac{\partial\delta v_x}{\partial y}\\ \dfrac{\partial\delta v_y}{\partial x} & \dfrac{\partial\delta v_y}{\partial y}\end{pmatrix}\begin{pmatrix}x\\ y\end{pmatrix} + \mathrm{O}(x^2+y^2)\\ &= \begin{pmatrix}k+c & a-b\\ a+b & k-c\end{pmatrix}\begin{pmatrix}x\\ y\end{pmatrix} + \mathrm{O}(x^2+y^2).\end{aligned} \tag{10.18}$$

Here the partial derivatives are evaluated at the origin and a, b, c, k are linear combinations of the values of these derivatives – the reason for writing the partial-derivative matrix in this way will emerge shortly. We expect the mean radial velocity of the stars at $\mathbf{x} = (x, y)$ to be the projection of $\delta\mathbf{v}$ on to $\mathbf{x}$:

$$\begin{aligned}v_{\rm los} &= \frac{1}{d}\mathbf{x}\cdot\delta\mathbf{v}\\ &\simeq \frac{1}{d}\left[(k+c)x^2 + (k-c)y^2 + 2axy\right]\end{aligned} \tag{10.19}$$

where $d \equiv (x^2+y^2)^{1/2}$ is heliocentric distance as usual. In terms of Galactic longitude l, we have $x = d\cos l$ and $y = d\sin l$, so with the aid of two trigonometric identities equation (10.19) becomes

$$v_{\rm los} = d(k + c\cos 2l + a\sin 2l) + \mathrm{O}(d^2). \tag{10.20}$$

This equation suggests that we could determine the constants a, c and k by measuring the radial velocities of stars of similar distances and plotting the results as a function of longitude l. The stars could be selected to be stars of given spectral type and apparent magnitude, thus guaranteeing that they all have similar distances.

The constant b can be determined from the proper motions of stars. To see this, let δv_t be the component of velocity perpendicular to the line of sight. Then

$$\begin{aligned}\delta v_t &= \frac{1}{d}(\mathbf{x}\times\delta\mathbf{v})_z = \frac{1}{d}(x\delta v_y - y\delta v_x)\\ &= d(b + a\cos 2l - c\sin 2l) + \mathrm{O}(d^2).\end{aligned} \tag{10.21}$$

Hence from a plot of the proper motion $\mu_l = v_t/d$ as a function of l we can determine a, b and c.

The relations (10.20) and (10.21) above are completely general – they assume only that $\mathbf{v}_{\rm SR}$ varies smoothly in the solar neighborhood. What do they reduce to if we assume that the disk is in circular rotation with angular speed $\Omega(R)$? For this case, equation (9.3) gives an exact relation for $v_{\rm los}(l, R)$. To obtain a relation equivalent to equation (10.20), we need to Taylor expand the right-hand side of equation (9.3) in powers of d. On Taylor expanding $\Omega(R)$ to first order in $R - R_0$, equation (9.3) yields

$$\begin{aligned}v_{\rm los}(l, R) &\simeq \left.\frac{\mathrm{d}\Omega}{\mathrm{d}R}\right|_{R_0}(R-R_0)R_0\sin l\\ &= -2A(R-R_0)\frac{R_0}{R}\sin l,\end{aligned} \tag{10.22}$$

where **Oort's constant** A is defined by

$$A \equiv -\tfrac{1}{2}\left(R\frac{\mathrm{d}\Omega}{\mathrm{d}R}\right)_{R_0} = \tfrac{1}{2}\left(\frac{v_c}{R} - \frac{\mathrm{d}v_c}{\mathrm{d}R}\right)_{R_0}. \tag{10.23}$$

On neglecting d^2 in equation (9.16), we have

$$(R-R_0)(R+R_0) = R^2 - R_0^2 \simeq -2R_0 d\cos l, \tag{10.24}$$

so approximating $(R + R_0)$ by $2R_0$, we may write to first-order in d

$$(R - R_0) = -d\cos l. \tag{10.25}$$

Combining equations (10.22) and (10.25) we find

$$v_{\rm los} \simeq Ad\sin 2l. \tag{10.26}$$

This is equation (10.20) for the special case of circular rotation. Evidently in this case $c = k = 0$, and $a = A$ is given by equation (10.23).

To derive equation (10.21) for the case of circular rotation we have to go back to equation (9.1). We write

$$\begin{aligned}v_t &= \left(\frac{\mathbf{R}-\mathbf{R}_0}{|\mathbf{R}-\mathbf{R}_0|}\times\left[\boldsymbol{\Omega}(R)\times\mathbf{R} - \boldsymbol{\Omega}(R_0)\times\mathbf{R}_0\right]\right)_z\\ &= \left(\frac{\mathbf{R}-\mathbf{R}_0}{d}\times\left\{\boldsymbol{\Omega}(R)\times(\mathbf{R}-\mathbf{R}_0) + \left[\boldsymbol{\Omega}(R) - \boldsymbol{\Omega}(R_0)\right]\times\mathbf{R}_0\right\}\right)_z\\ &\simeq \Omega_z(R)d + \left.\frac{\mathrm{d}\Omega_z}{\mathrm{d}R}\right|_{R_0}\frac{(\mathbf{R}-\mathbf{R}_0)\cdot\mathbf{R}_0}{d}.\end{aligned} \tag{10.27}$$

Box 10.3: The AR_0 Formula

We can derive a useful formula from equation (9.4) for the terminal velocity (see §9.2.3) in the direction l by writing

$$\Omega(R_0\sin l) - \Omega(R_0) \simeq \left(\frac{\mathrm{d}\Omega}{\mathrm{d}R}\right)_{R_0} R_0(\sin l - 1) \quad \text{for} \quad l \simeq 90°. \qquad (1)$$

Substituting for $\mathrm{d}\Omega/\mathrm{d}R$ from (10.23), equation (9.4) becomes, to first order in $(1-\sin l)$,

$$v_{\rm los}^{(\rm t)}(l) = 2AR_0(1-\sin l) \quad \text{for} \quad l \simeq 90°. \qquad (2)$$

This formula is useful because it links two quantities that are key but hard to measure accurately, A and R_0, to the terminal velocity curve, which can be measured quite accurately – see §9.2.1. Kerr & Lynden-Bell (1986) list several determinations of AR_0, and find that recent observations give $AR_0 = 108 \pm 3\,\mathrm{km\,s^{-1}}$. The data plotted in Figure 9.16 yield a rather larger value, $AR_0 \simeq 115\,\mathrm{km\,s^{-1}}$, but with considerable uncertainty.

By drawing the appropriate triangle it is easy to see that $(\mathbf{R}-\mathbf{R}_0)\cdot\mathbf{R}_0 = -dR_0\cos l$. When we substitute this relation and equation (10.25) into equation (10.27), we find

$$\begin{aligned} v_t &\simeq \Omega_z(R_0)d + dR_0\left.\frac{\mathrm{d}\Omega_z}{\mathrm{d}R}\right|_{R_0}\cos^2 l \\ &= d\Big(\Omega_z(R_0) + \tfrac{1}{2}R_0\left.\frac{\mathrm{d}\Omega_z}{\mathrm{d}R}\right|_{R_0}(1+\cos 2l)\Big). \end{aligned} \qquad (10.28)$$

We now recall that, because the Milky Way rotates clockwise, $\Omega_z = -\Omega$, and define **Oort's constant** B by

$$\begin{aligned} B &\equiv -\Big(\Omega + \tfrac{1}{2}R\frac{\mathrm{d}\Omega_z}{\mathrm{d}R}\Big)_{R_0} \\ &= -\tfrac{1}{2}\left(\frac{v_c}{R} + \frac{\mathrm{d}v_c}{\mathrm{d}R}\right)_{R_0}. \end{aligned} \qquad (10.29)$$

Equation (10.28) then becomes

$$\mu_l = \frac{v_t}{d} = B + A\cos 2l. \qquad (10.30)$$

This is equation (10.21) for the case of circular rotation. Evidently in the case of circular rotation $b = B$ is given by equation (10.29).

A measures the **shear** in the disk at the Sun. It would be zero if the disk rotated like a solid body, such as a compact disk, for then Ω would be independent of radius and, by equation (10.23), A would vanish. B measures the **vorticity** of the material of the disk, that is, its tendency to circulate about any given point – see Problem 10.8. From equations (10.23) and (10.29) it immediately follows that

$$v_c = R_0(A-B) \quad \text{and} \quad \left.\frac{\mathrm{d}v_c}{\mathrm{d}R}\right|_{R_0} = -(A+B). \qquad (10.31)$$

In §8.2.4 we saw that the circular-speed curves of spirals are flat or gently rising at large radii. If the Milky Way's circular speed curve followed this pattern at the Sun, we would have $A + B \lesssim 0$.

Estimating the Oort constants Kuijken & Tremaine (1991) reviewed the observational constraints on c and k, and concluded that

$$c = 0.6 \pm 1.1\,\mathrm{km\,s^{-1}\,kpc^{-1}}, \qquad k = -0.35 \pm 0.5\,\mathrm{km\,s^{-1}\,kpc^{-1}}. \qquad (10.32)$$

Thus these two constants are zero to within the errors, just as they should be if the Milky Way is axisymmetric. In view of this result, we shall assume that $a = A$ and $b = B$, and henceforth make no distinction between these logically distinct entities.

A can be determined either from radial velocities [equation (10.20)], or from proper motions [equation (10.21)]. Since the determination of $v_c(R_0)$ is one of the harder problems in Galactic structure, equation (10.23) is usually used to determine $v_c(R_0)$ from A rather than vice versa. Notice that the value of A derived from radial velocities is inversely proportional to the assumed distances d of the observed stars, and must be updated whenever there is an improvement in the accuracy of the standard distance scale.

Fundamentally, B can only be obtained from proper motions. Traditionally, equation (10.21) has been used. The great drawback of this technique is that any rotation of one's astrometric system (§2.1.5) will directly contribute to the measured value of B. To show this, we suppose that our astrometric system rotates at angular velocity $\boldsymbol{\omega}$, and calculate the contribution $\delta\mu_l$ that this rotation makes to the left-hand side of equation (10.21). The rotation of the system adds $\hat{\mathbf{x}}\times\boldsymbol{\omega}$ to the measured proper motion of a star that lies in the direction $\hat{\mathbf{x}}$. We wish to calculate the component of this proper motion that is perpendicular to the normal to the Galactic plane, $\hat{\mathbf{z}}$. This component is

$$\hat{\mathbf{z}}\times[(\hat{\mathbf{x}}\times\boldsymbol{\omega})\times\hat{\mathbf{z}}] = (\hat{\mathbf{z}}\cdot\hat{\mathbf{x}})\,\hat{\mathbf{z}}\times\boldsymbol{\omega} - (\hat{\mathbf{z}}\cdot\boldsymbol{\omega})\,\hat{\mathbf{z}}\times\hat{\mathbf{x}}. \qquad (10.33)$$

For stars that lie within the plane, $\hat{\mathbf{z}}\cdot\hat{\mathbf{x}} \simeq 0$ and $\hat{\mathbf{z}}\times\hat{\mathbf{x}}$ is just the unit vector in direction of increasing longitude l. Hence

$$\delta\mu_l = -\hat{\mathbf{z}}\cdot\boldsymbol{\omega}, \qquad (10.34)$$

which is obviously independent of l. However, in equation (10.21), B is precisely the term that is independent of l, so rotation of one's astrometric system directly affects the measured value of B. Moreover B is small; expressed in sensible units (like A and the Hubble constant it is a frequency) its value is $\simeq -4 \times 10^{-16}\,\mathrm{Hz}$. So one has to be *very* sure that one's frame is not rotating before reporting a measurement of B! It is a tribute to the diligence of astronomers that the errors in astrometric systems such as the FK5 that are based on the dynamics of the solar system (§2.1.5), are only of this order. Even so, values of B that are based upon an extragalactic system such as the ICRS (§2.1.5) are clearly to be preferred.

Kerr & Lynden-Bell (1986) reviewed the observational constraints on A and B and concluded that

$$A = 14.4 \pm 1.2\,\mathrm{km\,s^{-1}\,kpc^{-1}}, \qquad B = -12.0 \pm 2.8\,\mathrm{km\,s^{-1}\,kpc^{-1}}. \quad (10.35)$$

From the proper motions of Cepheids that were measured by the Hipparcos satellite (§2.1.3), Feast & Whitelock (1997) found

$$A = 14.8 \pm 0.8\,\mathrm{km\,s^{-1}\,kpc^{-1}}, \qquad B = -12.4 \pm 0.6\,\mathrm{km\,s^{-1}\,kpc^{-1}}. \quad (10.36)$$

Since Hipparcos measured proper motions on the ICRS, these estimates are the most reliable values of the Oort constants, and should supersede all earlier values. Since $A > |B|$ they imply a gently falling circular-speed curve at R_0. Numerically, $v_c(R_0) = 218(R_0/8\,\mathrm{kpc})\,\mathrm{km\,s^{-1}}$.

Recently an intriguing alternative to equation (10.21) has arisen, namely measurement by the VLA of the proper motion of the compact radio source Sgr A*, which is generally thought to mark the Galactic center (§9.5). Radio observations at seven epochs between 1981 and 1994 of the position of Sgr A* relative to extragalactic sources show that it has proper motion (Backer 1996)

$$(\mu_l, \mu_b) = (-6.55 \pm 0.17, -0.48 \pm 0.12)\,\mathrm{mas\,yr^{-1}}. \quad (10.37)$$

This proper motion is the sum of the proper motion of Sgr A* with respect to the Galactic center and the reflex of the Sun's velocity, which is itself the sum of $v_c(R_0)$ and the solar motion with respect to the LSR. When we subtract the contribution of the latter for $R_0 = 8\,\mathrm{kpc}$, we are left with $(\mu_l', \mu_b') = (-6.24 \pm 0.17, -0.30 \pm 0.12)\,\mathrm{mas\,yr^{-1}}$. Clearly μ_b' must reflect the intrinsic motion of Sgr A*, and the fact that it does not differ significantly from zero encourages us to believe that Sgr A* is essentially stationary with respect to the Galactic center. In this case, from the first of equations (10.31) it follows that

$$\mu_l' = A - B = 30.1 \pm 0.8\,\mathrm{km\,s^{-1}\,kpc^{-1}}, \quad (10.38)$$

which is marginally inconsistent with equation (10.36).

10.4 The structure of the stellar disk

In the last section we saw that different spectral types have characteristically different velocity dispersions. The discovery of this and related correlations in the 1950s constituted one of the major advances in our understanding of the structure and history of the Milky Way. In this section we investigate these correlations in detail and explore their implications for Galactic structure and evolution.

We speculated above that the correlations between spectral type and kinematics might be connected with the different mean ages of stars of different spectral types. We now pursue this hint by looking at samples of stars to which ages can be assigned.

10.4.1 Ages and metallicities of nearby stars

The stars which can most readily and reliably be assigned ages are dwarfs of MK type G and earlier: such a star begins to turn off the ZAMS within 10 Gyr (§5.1), and as it moves away from the ZAMS it can be dated from its position in the CM diagram. Moreover, an interesting upper limit can be placed on the age of any such star that is still on the ZAMS. For our present purposes, F and G stars are most interesting because their lifetimes are comparable to the long time-scales characteristic of Galactic evolution.

Edvardsson *et al.* (1993) report the results of a major study of such objects. They obtained high-quality spectra and space velocities for 189 nearby F and G dwarfs. By fitting sophisticated model atmospheres to their spectra they obtained for each star an age and the abundances of the elements O, Na, Mg, Al, Si, Ca, Ti, Fe, Ni, Y, Zr, Ba and Nd. From §5.2.1 we recognize Na and Al as odd-light elements, Mg, Si and Ca as α elements, Ti, Fe and Ni as iron-peak elements and Y, Zr, Ba and Nd as s-process elements. Their sample of stars was selected by searching a large catalog of stars with Strömgren *uvbyβ* photometry (§2.3.2) for stars of appropriate spectral type and age. Consequently, no inferences can be drawn from their results concerning the *fractions* of stars that have given ages or abundances, but currently they provide some of the best information regarding the mutual dependencies between abundances, velocity dispersion and age.

Correlations between abundances The left-hand panel of Figure 10.16 demonstrates that the abundances of the light and heavy s-process elements Y and Ba are tightly correlated, as theory predicts. The right-hand panel of Figure 10.16 shows that the abundances of secondary elements such as Ba increase faster than those of primary elements such as Mg – the slope of the mean relation in this panel implies that the abundance of Ba varies as the abundance of Mg to the power 1.7. In §5.2.1 we argued that, in the absence of neutron poisons, the slope of this relation would be 2, and will be smaller if poisons are present. Therefore a slope of 1.7 is entirely consistent with theory.